INTERNATIONAL JOURNAL FOR NUMERICAL METHODS IN FLUIDS
Int. J. Numer. Meth. Fluids 2002; **38**:407–427 (DOI: 10.1002/fld.223)

Gas-assisted fluid displacement in a circular tube and a rectangular channel

Fethi Kamişli*,† and Michael E. Ryan

Department of Chemical Engineering, State University of New York at Buffalo, Amherst, NY 14260, U.S.A.

SUMMARY

In this paper the amount of liquid left inside of a circular tube and a rectangular channel when displaced by another immiscible fluid are determined by solving the full creeping-motion equations. The exact continuity of stress on the free surface is employed with a finite difference method. In order to solve the equations, the steady-state shape of the interface is guessed and the normal stress boundary condition is dropped. The equations based on a stream function-vorticity formulation are solved with the aid of elliptic grid generation. The computed results are compared with the experimental results of Taylor (*J. Fluid Mech*. 1961; **10**:161), the theoretical results of Reinelt and Saffman (*SIAM J. Sci. Stat. Comput*. 1985; **6**:542) and our experimental data. The computed results are in close agreement with our experimental data and those of previous investigators. Copyright © 2002 John Wiley & Sons, Ltd.

KEY WORDS: Two-phase flow; gas–liquid displacement, gas-assisted flow

INTRODUCTION

The motion of long bubbles into Newtonian fluids confined in horizontal cylindrical tubes or channels of rectangular cross-section (Hele–Shaw cell) has been studied for several years. When a less viscous fluid displaces a more viscous fluid from the gap between two closely spaced parallel plates, the interface develops a tongue-like shape with the less viscous fluid penetrating into the more viscous fluid. Similarly, when air is forced into one end of a circular tube containing a viscous liquid, it forms a round-ended column or bullet-like shape which travels down the tube forcing some liquid out at the far end and leaving a fraction of the liquid m, in the form of an annular layer covering the wall. In the case of a square channel the shape of the less viscous fluid penetrating into the more viscous fluid depends on the velocity of the penetrating fluid. If the velocity of the penetrating fluid (called the bubble or finger hereafter) is larger than a certain limiting value, the bubble assumes a bullet-like shape; otherwise, the bubble conforms to the shape of the square channel. In a rectangular channel, if the capillary number, $Ca = \mu u_b/\sigma$ is not too large, a single steady-state tongue-like

*Correspondence to: F. Kamişli, Department of Chemical Engineering, Faculty of Engineering, University of Firat, 23279 Elaziğ, Turkey.
†E-mail: fkamisli@firat.edu.tr

Received 17 December 1998
Revised 10 May 2000

shape moves through the cell with constant velocity u_b, where μ is the dynamic viscosity of the driven liquid, u_b is the bubble velocity, and σ is the gas–liquid interfacial tension. In a circular tube or square channel the bullet-like shape of the bubble persists even at very large capillary number. In other words, the fingering effect does not occur in the case of a long bubble advancing in either a circular tube or a square channel at large capillary numbers.

Fairbrother and Stubbs [1] performed the first experiments to determine the amount of liquid left inside of a tube when it is displaced by another immiscible fluid. They determined the flow rate of the liquid by measuring the motion of the gas interface in the tube. When the tube is not completely filled with the liquid, the gas interface will move faster than the average velocity of the liquid due to the deposition of a thin film of liquid on the walls of the tube and if the tube is long enough, blowout will take place somewhere within the tube. An empirical correlation for the fraction of the liquid deposited on the walls of the tube was formulated as follows:

$$m = (u_b - u)/u_b = 1.0Ca^{1/2} = (\mu u_b/\sigma)^{1/2}$$

where u is mean velocity of fluid ahead of the bubble. This result was found satisfactory for capillary numbers between 10^{-3} and 10^{-2}.

Isothermal gas-assisted displacement of Newtonian liquids in circular tubes was also experimentally studied by Taylor [2]. By plotting the fraction of the liquid as a function of the capillary number, he collapsed the data onto a single curve, and showed that this fraction asymptotically approached the value of 0.56 for a capillary number nearly equal to two. Cox [3, 4] extended Taylor's [2] result to capillary numbers up to 10 and showed that the limiting fraction of the liquid deposited on the walls of the tube was approximately 0.6. His theoretical analysis resulted in a fourth-order differential equation in terms of the stream function. Inertial and gravitational forces were neglected. The streamlines were assumed to be a specific function of the spatial coordinates. The governing equations were expressed in matrix form and solved numerically.

Bretherton [5] also undertook a theoretical analysis of this problem for circular capillaries. He found an approximate solution to this problem for a circular cross-section by the method of matched asymptotic expansions. The idea behind this theoretical treatment is that for sufficiently small *Ca* the viscous stresses appreciably modify the static profile of the bubble only very near to the wall. In this region *the lubrication approximation* gives a good description of the flow field and of the interface profile. In the center of the capillary, the static profile is valid and there is a region of overlap in which the two solutions are matched. Using the lubrication approximation which requires quasi-unidirectional flow in the thin liquid film and assuming the slope of the fluid–fluid interface to be small, it can be shown that the velocity profile is parabolic. The boundary conditions for steady flow are the no slip condition at the capillary wall, and tangential stress equal to zero at the fluid interface. The bubble is assumed to be inviscid resulting in a constant pressure within the bubble. The pressure in the liquid film is given by the pressure drop across the interface which is approximated by the Young–Laplace equation. Bretherton [5] also systematically explored a number of possible causes for the discrepancy between the analysis and experimental data. However, none of these could provide a satisfactory explanation. Schwartz *et al.* [6] considered the same problem and found some differences in liquid film thickness for sufficiently long bubbles, as compared to short bubbles.

Another experimental study by Marchessault and Mason [7] used air bubbles in a dilute aqueous solution of potassium chloride. Film thicknesses were inferred from resistance measurements and were found to be substantially larger than those reported by Bretherton [5]. The residual wetting layer of the displaced liquid will vary with the velocity of advance of the interface. Park and Homsy [8] demonstrated that the two-dimensional version of the Bretherton [5] problem is an appropriate local solution to describe the phenomenon.

Numerical studies of capillary-tube displacement of a wetting liquid by a semi-infinite inviscid slug of gas have been presented. Both Reinelt and Saffman [9] using a finite-difference method and Shen and Udell [10] using a finite element approach solved the full creeping-motion equations with the continuity of stress imposed exactly on the free surface. Reinelt and Saffman [9] obtained a numerical solution that is in close agreement with experimental data for a Newtonian liquid. They investigated the fraction of the liquid deposited on the walls of a channel as well as a circular tube, as a function of the capillary number. The Navier–Stokes equation was expressed in terms of the stream function and vorticity in order to solve the problem numerically.

Ratulowski and Chang [11] investigated a single discrete bubble and the motion of a long bubble in a circular tube and square channel. They determined the fraction of liquid deposited on the walls of the tube or channel and the pressure drop across the bubble front. According to their study, a single isolated bubble resembles an infinitely long bubble in terms of determining the film thickness and pressure drop across the bubble front if the length of the bubble exceeds the channel width. Their analysis is only valid for $Ca > 3 \times 10^{-3}$.

Kolb and Cerro [12] studied the isothermal gas-assisted displacement of a Newtonian liquid from a channel of square cross-section and showed that the liquid deposited on the wall of the square tube also approaches an asymptotic limit at high capillary numbers. Above $Ca = 0.1$ the gas forms a circular hollow core and thicker liquid deposition; below $Ca = 0.1$ the hollow core takes on the square cross-section of the tube as the deposition thickness is reduced. The above study was extended (Kolb and Cerro [13]) by adding *the lubrication approximation* for intermediate to large capillary numbers where the flow is axisymmetric. In their work the film thickness on the walls of the square channel can be predicted as a function of capillary number since the velocity profile of the fluid flowing between the bubble and the square channel walls is known. It was claimed that *the lubrication approximation* solution is in good agreement with experimental data for values of capillary number between 0.7 and 2.0.

Unlike previous investigators, Poslinski *et al.* [14] investigated non-Newtonian fluids deposited on the walls of a tube. They found that the fraction of the non-Newtonian fluid deposited on the walls is less than that of a corresponding Newtonian fluid at low capillary number. At higher capillary number the fraction of the liquid deposited asymptotically increases and approaches a value of 0.58.

Ro and Homsy [15] performed an asymptotic analysis of the gas-assisted displacement of a non-Newtonian fluid in a Hele–Shaw cell. The effects of normal stress and shear stress thinning in determining the film thickness and the pressure jump across the interface were examined. Viscoelastic fluids were modeled by an Oldroyd-B constitutive equation and the solutions for the constant film thickness region and the static meniscus region were matched in the transition regime as for the Newtonian case (see Park and Homsy [8]).

The planar geometry or Hele–Shaw cell consists of two closely separated parallel plates having a distance $2d$ between them. The sides of this rectangular channel are at a distance

$2Z_o$ apart where $d \ll Z_o$. Parameter λ is defined as (thickness of gas bubble)/(distance between the plates). For the cylindrical tube λ is defined as (diameter of the bubble)/(diameter of the tube). In the rectangular channel the thickness of the tongue-like shape is $2\lambda d$ and its width is $2\lambda_w Z_o$, where the parameter λ_w is equal to (width of the bubble)/(width of the rectangular channel).

The determination of the value of λ and λ_w has been a subject of much interest. The determination of λ_w as a function of capillary number, Ca, for different cell aspect ratios, Z_o/d, has been examined experimentally by Saffman and Taylor [16], Pitts [17], and Tabeling *et al.* [18]. Saffman and Taylor [16] and Pitts [17] found that the value of λ_w decreases monotonically to 0.5 when the bubble velocity is increased. In contrast, Tabeling *et al.* [18] reported that the value of λ_w never decreases to 0.5 when the bubble velocity is increased. The problem was reconsidered by McLean and Saffman [19] by including surface tension effects due to the lateral curvature of the interface of the advancing finger. In their numerical study the value of λ_w was close to 0.5 at large bubble velocity which is in good agreement with the experimental data. At low velocities (i.e. $C_b < 100$), the agreement with experiment was ambiguous since the finger sizes predicted by the theory were significantly below those actually measured, where

$$C_b = 12Ca(Z_o/d)^2$$

They found that the incorporation of surface tension and cell aspect ratio did not remedy or reduce the disagreement between theory and experiment in terms of calculating the value of λ_w as a function of C_b. The approach of Bretherton [5] was reconsidered by Park and Homsy [8] in the horizontal Hele–Shaw cell at very low capillary number. The problem was solved using a perturbation method with an asymptotic expansion of $Ca^{1/3}$ and the ratio of the gap width to the transverse characteristic length $\delta_e = d/Z_o$ as small quantities. They obtained relationships between λ, Ca, and δ_e for calculating the film thickness and pressure jump across the bubble front. The resulting expressions were compared with the results of Bretherton [5] and Landau and Levich [20] and were considered to give improved results.

Reinelt [21] extended his earlier work by determining the perturbation solution of the axisymmetric flow problem for small values of Ca and $\delta = d/R$. In his study, some of the boundary conditions were improved by incorporating the film thickness into the kinematic boundary condition and taking into account the dependence of Δp on the capillary number. The problem was also numerically solved using a conformal mapping method and the numerical results were presented in another paper (Reinelt [22]). Although the inclusion of the effects of the film thickness variation and the lateral and transverse curvature on the interface boundary conditions improved the quantitative agreement between the experimental and numerical results, it did not remove the discrepancy associated with different finger widths.

Other relevant literature pertains to applications that are related to gas–liquid flows through porous media and in process equipment, cavitation in the narrow passages of bearings, and the coating of monolithic structures for the manufacture of automotive catalytic converters (Saffman and Taylor [16], Taylor [23], Fernandes *et al.* [24], and Kolb *et al.* [25]).

In this paper a different numerical approach is developed to solve the free surface problem and it is applied to the gas-assisted liquid displacement in the circular tube and Hele–Shaw cell. The stream function, vorticity and treatment of some of the boundary conditions used in this paper were also used by Reinelt and Saffman [9]. However, Reinelt and Saffman

used a chimera mesh (cartesian and curvilinear) in order to solve the problem. Unlike a chimera mesh, in this paper, a unique elliptic grid is used to overcome this difficulty. Also the problem is examined experimentally in order to determine the effect of non-Newtonian fluid rheology such as shear thinning and viscoelasticity on the liquid fraction deposited on the wall as a function of capillary number (see Kamişli [26]). However, the experimental results are not presented here except for the residual liquid film thickness of Newtonian and some non-Newtonian fluids as a function of capillary number.

EXPERIMENTAL

The experimental arrangement consists of a gas supply tank, pressure transducer, transparent plastic or glass tubes/channels and associated valves and fittings as shown in Figure 1. The volume of the gas supply tank was chosen to be very large in comparison to the volume of the gas within the tube or channel in order to minimize pressure fluctuations during the experiments. Pressurized air was used as the gas and was supplied by a local compressed air line and monitored with a pressure gauge mounted on the tank. The desired pressure level can be accurately adjusted by keeping valve B open and D closed and reading the pressure from the pressure transducer for a particular setting of valve C. The line pressure is also independently measured using a pressure transducer situated close to the channel assembly. Plastic or glass tube having diameter 4.763 mm and a length of 50 cm were used. Caliper measurements showed that the inner radius along the tube length had a maximum variation of ± 0.065 mm.

Isothermal experiments have been conducted to measure the displacement of gas–liquid interface as a function of the applied pressure differential. The velocity of the interface and the residual liquid film thickness have been determined for Newtonian, non-Newtonian, and viscoelastic liquids (see Kamişli [26] for detail). Viscosity was measured using a Haake Rotovisco (Model RV12) as well as a calibrated glass capillary viscometer. Experiments were performed in two types of tube arrangement, namely open tubes and valve-mounted closed tubes. In the tube open to the atmosphere, the tube was initially filled with liquid to a distance of 15 cm. The end of the tube was open to the atmosphere. The velocity of the gas bubble and displaced liquid were determined using a stop-watch and observed positions of the gas–liquid interface. The moving bubble attained its final shape within a few

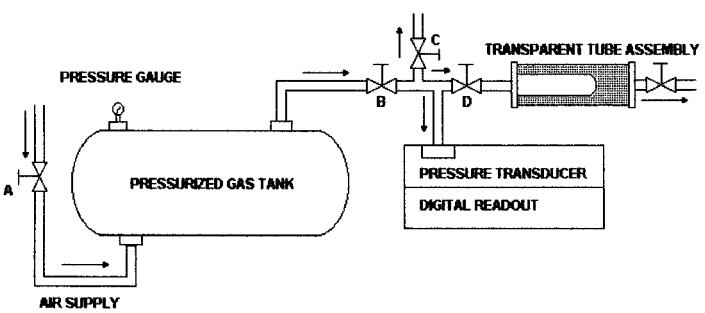

Figure 1. Schematic diagram of the experimental apparatus.

diameters of the gas injection point and translated unchanged along the length of the tube. The velocity of the gas bubble and the velocity of the liquid displaced by the gas are dependent upon how much liquid there is between the nose of the bubble and the moving liquid front.

On the other hand, the valve-mounted closed tubes result in a uniform bubble velocity since the flow resistance of the fluid in channel is negligible when compared with the resistance valve. In this type of arrangement experiments were conducted using a completely filled tube. The maximum variation in the bubble velocity was found to be less than 5 per cent for most of the test fluids. The capillary numbers were calculated from the average bubble velocity. In this case, the fraction of liquid deposited on the tube wall was calculated by weighing the liquid expelled by the long gas bubble since the initial amount of liquid within the tube is known from the liquid density, tube diameter, and length.

In this paper, the results of valve-mounted closed tubes were presented in order to compare with the results of numerical solution since the velocity in the numerical solution was taken to be uniform along the axial direction.

RESULTS OF EXPERIMENT

The fraction of the liquid deposited on the wall of the tube for the different liquids is plotted in Figure 2 as a function of the capillary number. The experimental data for the Newtonian fluid are in close agreement with Taylor's [2] experimental data as can be seen in Figure 2. Different capillary numbers for each tube are obtained by changing the pressure of the gas. Each experiment was repeated six times in order to check repeatability. The coating of the liquid on the walls of the tube depends primarily on how fast the gas moves through

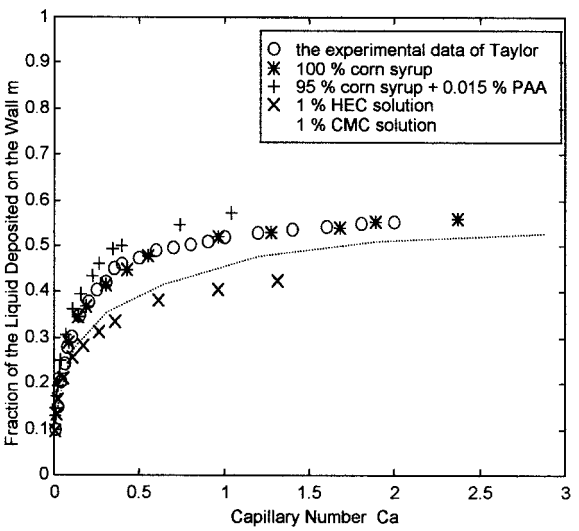

Figure 2. The fraction of the liquid deposited on the wall (m) versus *Ca* for Newtonian and non-Newtonian fluids.

the liquid. Increasing gas pressure, larger radii and lower viscosity reduce the flow resistance and result in higher bubble velocity and higher residual liquid film thickness on the tube wall.

Numerical approach

Finite difference techniques have been extensively used for the simulation of a wide spectrum of flow situations since the finite difference approach possesses inherent simplicity of formulation and ease of mesh refinement. For problems involving fluids described by complex constitutive relationships, it was deemed appropriate to develop a simple, efficient, finite difference scheme capable of solving steady free surface flows, in particular gas-assisted fluid displacement. Reinelt and Saffman [9] have solved this problem for a Newtonian fluid by using a finite difference approach.

Apart from the difficulties associated with the unknown shape and location of the free surface, another problem arises from the surface boundary conditions which are expressed in terms of stresses. Traditionally, free surface calculations using either finite element or finite difference techniques have employed the velocity and pressure as the primitive variables. For steady flow problems, if the continuity equation is not solved directly along with the momentum equations, this primitive variable formulation poses considerable difficulties in satisfying the mass conservation requirement. If the stream function and vorticity formulation is employed, mass continuity is satisfied identically but difficulties are encountered in enforcing the free surface boundary conditions involving pressure explicitly. Although pressure could be eliminated by differentiation and algebraic manipulation of the momentum equations in order to remove the pressure gradient, the numerical evaluation of third-order derivatives of the stream function at the boundary becomes necessary.

The present method, which is based on a stream function and vorticity formulation, obviates the need for this numerically inaccurate operation. Instead, quasi-linearized forms of the stress boundary conditions are employed in order to determine the variable values at the interface. One difficulty associated with this problem is the presence of a singularity and an undetermined function for the derivative of pressure at the nose of the bubble. Although the velocity in the axial direction is finite, the velocity in the radial direction is equal to zero as x goes to zero. Therefore the problem should be handled in a different manner at the origin. In order to eliminate the undetermined function L'Hopital's rule can be applied.

In this paper, the penetration of a gas bubble into an initially filled liquid region consisting of a Newtonian fluid is considered. It is assumed that the viscosity of the gas is negligible compared with that of the liquid. It is also assumed that gravitational and inertial forces are small in comparison with the viscous forces. However, there is no difficulty incorporating the effect of gravity and inertia with the method presented here. Two different geometries are considered, namely planar and cylindrical.

Mathematical formulation of the two-dimensional and axisymmetric flow problem

Consider the motion of a gas bubble into an incompressible Newtonian liquid as shown schematically in Figure 3. For convenience, velocities are non-dimensionalized by the uniform velocity u_b, the transverse and axial coordinates by the characteristic length d, and the pressure by σ/d. The characteristic length d is taken to be either the radius of the tube or half of the distance between the parallel plates. The equation of continuity and motion are given

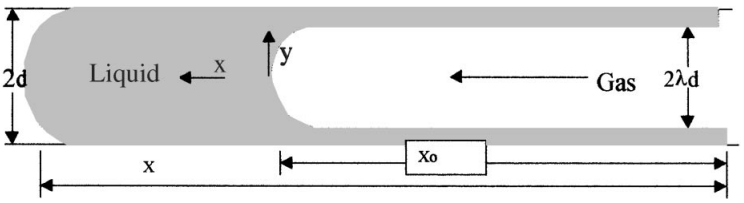

Figure 3. Schematic diagram of the gas-assisted displacement.

as follows:

$$\frac{1}{\dot{y}^a}\frac{\partial}{\partial \dot{y}}(\dot{y}^a \dot{u}) + \frac{\partial \dot{v}}{\partial \dot{x}} = 0 \tag{1}$$

$$\rho\left(\frac{\partial \dot{v}}{\partial \dot{t}} + \dot{v}\frac{\partial \dot{v}}{\partial \dot{x}} + \dot{u}\frac{\partial \dot{v}}{\partial \dot{y}}\right) = -\frac{\partial \dot{p}}{\partial \dot{x}} + \left[\frac{1}{\dot{y}^a}\frac{\partial}{\partial \dot{y}}(\dot{y}^a T_{xy}) + \frac{\partial T_{xx}}{\partial \dot{x}}\right] \tag{2}$$

$$\rho\left(\frac{\partial \dot{u}}{\partial \dot{t}} + \dot{v}\frac{\partial \dot{u}}{\partial \dot{x}} + \dot{u}\frac{\partial \dot{u}}{\partial \dot{y}}\right) = -\frac{\partial \dot{p}}{\partial \dot{y}} + \left[\frac{1}{\dot{y}^a}\frac{\partial}{\partial \dot{y}}(\dot{y}^a T_{yy}) + \frac{\partial T_{yx}}{\partial \dot{x}}\right] \tag{3}$$

The parameter a has a value of either 0 or 1 depending on the geometry (0 corresponds to the planar case and 1 corresponds to a cylindrical geometry). T_{ij} is the viscous part of the stress tensor and $\dot{p}$ is the pressure. The velocity components $\dot{\mathrm{v}}$ and $\dot{\mathrm{u}}$ are in the $\dot{x}$ and $\dot{y}$ directions, respectively. The $\dot{y}$ axis is taken normal to the channel plates (or tube wall) with the origin at the mid-plane (or tube axis). Thus $\dot{\mathrm{y}}$ has the value of $\pm d$ for the planar case (or d for the cylindrical case) at the solid boundaries. The nose of the bubble moves along the negative $\dot{x}$ axis. The origin is assumed to be located at the nose of the bubble and consequently the velocity is independent of time with respect to this frame of reference. Dimensionless variables are defined as follows:

$$x = (\dot{\mathrm{x}} - u_b \dot{t})/d, \quad y = \dot{\mathrm{y}}/d, \quad R = \dot{R}/d$$
$$v = \dot{\mathrm{v}}/u_b, \quad u = \dot{\mathrm{u}}/u_b, \quad p = \dot{p}/(\sigma/d)$$

In terms of these dimensionless variables Equations (1)–(3) (neglecting inertia) become

$$\frac{1}{y^a}\frac{\partial}{\partial y}(y^a u) + \frac{\partial v}{\partial x} = 0 \tag{4}$$

$$\frac{\partial p}{\partial y} = Ca\left[\frac{\partial}{\partial y}\left(\frac{1}{y^a}\frac{\partial}{\partial y}(y^a u)\right) + \frac{\partial^2 u}{\partial x^2}\right] \tag{5}$$

$$\frac{\partial p}{\partial x} = Ca\left[\frac{1}{y^a}\frac{\partial}{\partial y}\left(y^a \frac{\partial v}{\partial y}\right) + \frac{\partial^2 v}{\partial x^2}\right] \tag{6}$$

where the capillary number Ca is the ratio of the viscous force to the force due to surface tension. Incompressibility implies the existence of a stream function ψ, defined as

$$u = -\frac{1}{y^a}\frac{\partial \psi}{\partial x}, \quad \text{and} \quad v = \frac{1}{y^a}\frac{\partial \psi}{\partial y} \tag{7}$$

The vorticity ω, is defined as

$$\omega = \frac{\partial u}{\partial x} - \frac{\partial v}{\partial y} \tag{8}$$

Substituting Equation (7) into Equation (8) yields

$$\frac{\partial^2 \psi}{\partial x^2} + \frac{\partial^2 \psi}{\partial y^2} - \frac{a}{y}\frac{\partial \psi}{\partial y} = -y^a \omega \tag{9}$$

After eliminating pressure from the equations of motion, the vorticity transport equation is given by

$$\frac{\partial^2 \omega}{\partial x^2} + \frac{\partial^2 \omega}{\partial y^2} + \frac{a}{y}\frac{\partial \omega}{\partial y} - \frac{a}{y^2}\omega = 0 \tag{10}$$

In addition, the pressure gradients are related to the vorticity by means of the following relationships

$$\begin{aligned} \frac{\partial p}{\partial x} &= -Ca\left[\frac{a}{y}\omega + \frac{\partial \omega}{\partial y}\right] \\ \frac{\partial p}{\partial y} &= Ca\frac{\partial \omega}{\partial x} \end{aligned} \tag{11}$$

The appropriate boundary conditions at the interface for the present flow problem are formulated as follows:

Since the free surface represents a streamline, the surface gradient dy/dx is related to the surface velocity components by the kinematic boundary condition

$$\frac{dy}{dx} = \frac{u}{v} \tag{12}$$

Along the free surface the stress component tangential to the free surface must vanish.

Thus, at $y = y(x)$, $0 < x \leqslant +\infty$

$$\left[1 - \left(\frac{dy}{dx}\right)^2\right]\tau_{xy} + \frac{dy}{dx}(\tau_{yy} - \tau_{xx}) = 0 \tag{13}$$

The normal stress component must be balanced by the tractions due to surface tension forces and the pressure exerted on the surface by the bubble (gas). Therefore

$$\frac{1}{\left\{1 + \left(\frac{dy}{dx}\right)^2\right\}}\left[\tau_{yy} + \left(\frac{dy}{dx}\right)^2 \tau_{xx} - 2\frac{dy}{dx}\tau_{yx}\right] = -\dot{p}_0 + \frac{\sigma}{\dot{R}} \tag{14}$$

where $\dot{p}_o$ is the bubble pressure and $\dot{R}$ is the total radius of curvature at the interface given by

$$\frac{1}{R} = \frac{d^2y}{dx^2}\left[1+\left(\frac{dy}{dx}\right)^2\right]^{-3/2} - \frac{a}{y}\left[1+\left(\frac{dy}{dx}\right)^2\right]^{-1/2} \tag{15}$$

Since y is a positive term and $[(d^2y)/(dx^2)]$ a negative one, the $1/R$ in Equation (14) was taken with absolute value in order to get correct expression.

τ_{ij} is the total stress and is defined as

$$\tau_{ij} = -\dot{p}\delta_{ij} + \mu\left(\frac{\partial \dot{v}_i}{\partial \dot{x}_j} + \frac{\partial \dot{v}_j}{\partial \dot{x}_i}\right)$$

where

$$\delta_{ij} = \begin{cases} 0 & \text{if } i \neq j \\ 1 & \text{if } i = j \end{cases}$$

Since the gas pressure is constant, it is taken to be zero without any loss of generality. Since the free surface represents a streamline, it is arbitrarily chosen to be zero.

These three interface conditions can be rewritten in terms of the velocity and stream function as follows:

$$\psi = 0 \quad \text{and} \quad \frac{dy}{dx} = \frac{u}{v} \tag{16}$$

$$\omega = 2u_x + 2\frac{\dfrac{dy}{dx}}{\left\{1-\left(\dfrac{dy}{dx}\right)^2\right\}}(u_y - v_x) \tag{17}$$

$$p = -\frac{1}{R} + 2\frac{Ca}{\left[1+\left(\dfrac{dy}{dx}\right)^2\right]}\left\{u_y - \frac{dy}{dx}(v_y + u_x) + \left(\frac{dy}{dx}\right)^2 v_x\right\} \tag{18}$$

where the notation k_l indicates the derivative of k with respect to l. The boundary condition given by Equation (17) is obtained by combining Equations (8) and (13).

Coordinate transformation and numerical solution

The irregular physical domain (x, y) is transformed to a regular computational domain (ξ, η) by means of elliptic grid generation (Thompson *et al.* [27] and Hoffman and Chang [28]). This transformed domain $\xi_1 < \xi < \xi_2$ and $\eta_1 < \eta < \eta_2$ is chosen to be the computational field since the free surface becomes coincident with the η_1 boundary, thereby permitting the free surface conditions to be enforced directly and accurately at the boundary. Both the physical and computational domains are shown in Figure 4.

Consider the following transformation

$$x = x(\xi, \eta) \quad \text{and} \quad y = y(\xi, \eta) \tag{19}$$

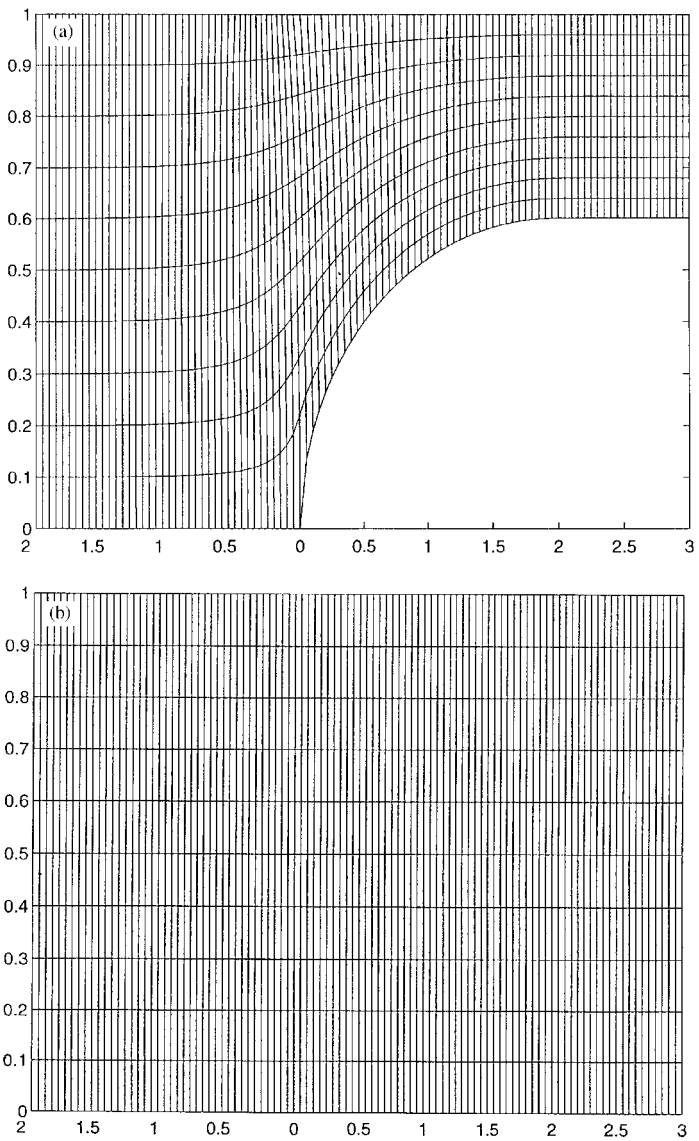

Figure 4. Schematic diagram of the restricted field in the (a) physical and (b) computational domain.

Therefore the Laplacian is given as follows

$$\frac{\partial^2}{\partial x^2}+\frac{\partial^2}{\partial y^2}=(\xi_x^2+\xi_y^2)\frac{\partial^2}{\partial \xi^2}+(\eta_x^2+\eta_y^2)\frac{\partial^2}{\partial \eta^2}+2(\eta_x\xi_x+\eta_y\xi_y)\frac{\partial^2}{\partial \xi\partial \eta}$$
$$+(\xi_{xx}+\xi_{yy})\frac{\partial}{\partial \xi}+(\eta_{xx}+\eta_{yy})\frac{\partial}{\partial \eta} \tag{20}$$

The elliptic grid generation implies that $\xi_{xx} + \xi_{yy} = 0$ and $\eta_{xx} + \eta_{yy} = 0$ and Equation (20) becomes

$$\frac{\partial^2}{\partial x^2} + \frac{\partial^2}{\partial y^2} = (\xi_x^2 + \xi_y^2)\frac{\partial^2}{\partial \xi^2} + (\eta_x^2 + \eta_y^2)\frac{\partial^2}{\partial \eta^2} + 2(\eta_x \xi_x + \eta_y \xi_y)\frac{\partial^2}{\partial \xi \partial \eta} \tag{21}$$

Conversely

$$\xi = \xi(x, y) \quad \text{and} \quad \eta = \eta(x, y)$$

and therefore

$$\begin{aligned} \xi_x &= J y_\eta; \quad \xi_y = -J x_\eta \\ \eta_y &= J x_\xi; \quad \eta_x = -J y_\xi \end{aligned} \tag{22}$$

where

$$J = \frac{1}{(x_\xi y_\eta - y_\xi x_\eta)}$$

Making use of these relationships in Equations (9) and (10) gives

$$\vartheta \frac{\partial^2 \psi}{\partial \xi^2} + \gamma \frac{\partial^2 \psi}{\partial \eta^2} + 2\beta \frac{\partial^2 \psi}{\partial \eta \partial \xi} - \frac{a}{y}\left(-x_\eta \frac{\partial \psi}{\partial \xi} + x_\xi \frac{\partial \psi}{\partial \eta}\right) = -\frac{y^a \omega}{J} \tag{23}$$

$$\vartheta \frac{\partial^2 \omega}{\partial \xi^2} + \gamma \frac{\partial^2 \omega}{\partial \eta^2} + 2\beta \frac{\partial^2 \omega}{\partial \eta \partial \xi} + \frac{a}{y}\left(-x_\eta \frac{\partial \omega}{\partial \xi} + x_\xi \frac{\partial \omega}{\partial \eta}\right) - \frac{a\omega}{y^2 J} = 0 \tag{24}$$

Similarly Equations (11), (16), (17) and (18) become

$$\begin{aligned} p_\xi &= Ca\left(-\frac{a}{y}\omega x_\xi - \beta \omega_\xi - \gamma \omega_\eta\right) \\ p_\eta &= Ca\left(-\frac{a}{y}\omega x_\eta + \vartheta \omega_\xi + \beta \omega_\eta\right) \end{aligned} \tag{25}$$

$$\frac{y_\xi}{x_\xi} = \frac{u}{v} \tag{26}$$

$$\omega = 2J(y_\eta u_\xi - y_\xi u_\eta) + \frac{J\left(\frac{y_\xi}{x_\xi}\right)}{\left[1 - \left(\frac{y_\xi}{x_\xi}\right)^2\right]}(x_\xi u_\eta - x_\eta u_\xi - y_\eta v_\xi + y_\xi v_\eta) \tag{27}$$

$$p = -\frac{1}{R} + \frac{2Ca\gamma\left[u_\eta - \frac{y_\xi}{x_\xi}v_\eta - \frac{\beta}{\gamma}\left(\frac{y_\xi}{x_\xi}v_\xi - u_\xi\right)\right]}{\left[x_\xi\left(1 + \left(\frac{y_\xi}{x_\xi}\right)^2\right)\right]} \tag{28}$$

where

$$\vartheta = J(y_\eta^2 + x_\eta^2)$$

$$\gamma = J(y_\xi^2 + x_\xi^2)$$

$$\beta = -J(x_\eta x_\xi + y_\eta y_\xi)$$

It is assumed that the shape of the bubble is symmetric about the mid-plane or tube axis and therefore it is sufficient to solve the problem over the region of positive y. The boundary conditions are given as:

At the inlet:

$$v = -\frac{a+3}{2}\lambda^{a+1}(1-y^2) + 1 \quad 0 \leqslant y \leqslant 1$$

$$\psi = -\frac{a+3}{2}\lambda^{a+1}\left(\frac{y^{a+1}}{a+1} - \frac{y^{a+3}}{a+3}\right) + \frac{y^{a+1}}{a+1} \quad 0 \leqslant y \leqslant 1$$

$$u = 0$$

$$\omega = -(3+a)\lambda^{a+1} y \quad 0 \leqslant y \leqslant 1 \quad x = -\infty$$

At the outlet

$$v(x, y) = 1 \quad \text{at } y = 1 \text{ as } x \to +\infty$$

$$\psi(x, y) = \frac{1}{a+1}(y^{a+1} - \lambda^{a+1})$$

$$\omega = 0$$

$$u = 0$$

At the axis or mid-plane

$$v(x, y) = -\left(\frac{a+3}{2}\right)\lambda^{a+1} + 1$$

$$\psi(x, 0) = 0$$

$$u(x, 0) = 0$$

$$\omega(x, 0) = 0$$

At the walls of the planar channel or tube

$$v(x, 1) = 1$$

$$\psi(x, 1) = \frac{1}{a+1}(1 - \lambda^{a+1})$$

$$u(x,1)=0$$

$$\omega(x,1)=-v_y=-\eta_y v_\eta$$

The governing relationships are expressed in terms of finite differences. Central differences (five-point formula) for interior grid points and three-point one-sided forward differences or three-point one-sided backward differences at the boundaries were used. These yield second-order accuracy. Thus the vorticity derivatives in terms of finite differences at the interior grid points are expressed as follows:

$$\omega_{\xi\xi}=\frac{(\omega_{i+1,j}+\omega_{i-1,j}-2\omega_{i,j})}{(\Delta\xi)^2}+0[(\Delta\xi)^2]$$

$$\omega_{\eta\eta}=\frac{(\omega_{i,j+1}+\omega_{i,j-1}-2\omega_{i,j})}{(\Delta\eta)^2}+0[(\Delta\eta)^2]$$

$$\omega_{\xi}=\frac{(\omega_{i+1,j}-\omega_{i-1,j})}{2\Delta\xi}+0[(\Delta\xi)^2]$$

$$\omega_{\eta}=\frac{(\omega_{i,j+1}-\omega_{i,j-1})}{2\Delta\eta}+0[(\Delta\eta)^2]$$

$$\omega_{\eta\xi}=\frac{(\omega_{i+1,j+1}-\omega_{i-1,j+1}-\omega_{i+1,j-1}+\omega_{i-1,j-1})}{4(\Delta\eta\Delta\xi)}$$

At the boundaries

$$\omega_{\xi}=\frac{(-3\omega_{i,j}+4\omega_{i+1,j}-\omega_{i+2,j})}{2\Delta\xi}+0[(\Delta\xi)^2]$$

or

$$\omega_{\xi}=\frac{(3\omega_{i,j}-4\omega_{i-1,j}+\omega_{i-2,j})}{2\Delta\xi}+0[(\Delta\xi)^2]$$

In terms of finite differences, Equation (24) becomes

$$\omega_{i,j}=\frac{1}{\left\{2\vartheta_{i,j}+2\gamma_{i,j}\left(\dfrac{d\xi}{d\eta}\right)^2+\dfrac{a_{i,j}(d\xi)^2}{y_{i,j}^2J_{i,j}}\right\}}\times\left[\begin{array}{l}\vartheta_{i,j}(\omega_{i+1,j}+\omega_{i-1,j})+\gamma_{i,j}\left(\dfrac{d\xi}{d\eta}\right)^2(\omega_{i,j+1}-\omega_{i,j-1})+\\ \dfrac{\beta_{i,j}}{2}\dfrac{d\xi}{d\eta}(\omega_{i+1,j+1}-\omega_{i-1,j+1}-\omega_{i+1,j-1}+\omega_{i-1,j-1})+\dfrac{a_{i,j}d\xi}{2y_{i,j}}\\ \left(-x_{\eta(i,j)}(\omega_{i+1,j}-\omega_{i-1,j})+\dfrac{d\xi}{d\eta}x_{\xi(i,j)}(\omega_{i,j+1}-\omega_{i,j-1})\right)\end{array}\right] \tag{29}$$

Similarly all other expressions can be written in finite difference form with second-order accuracy.

In order to solve this problem by means of elliptic grid generation the boundary encompassing the computational domain must be defined. Therefore the governing equations are solved in the restricted domain $x_{\min} < x < x_{\max}$ and $0 \leqslant y \leqslant 1$. The restricted domain is a region occupied by the liquid only.

It is assumed initially that the shape of the bubble is known. This assumed shape permits generation of the grid points in the computational domain. Since the shape of the bubble is prescribed, one of the interface boundary conditions can be neglected. Reinelt and Saffman [9] dropped the normal stress condition at the interface. This condition is also dropped in our calculations. The vorticity is calculated using Equation (29) at every interior grid point. The stream function is then calculated using Equation (23). The velocities are calculated from the relationships below and the data obtained from Equation (23) for interior grid points

$$\begin{aligned} v &= \frac{J}{y^a}(x_\xi \psi_\eta - x_\eta \psi_\xi) \\ u &= \frac{J}{y^a}(y_\xi \psi_\eta - y_\eta \psi_\xi) \end{aligned} \tag{30}$$

ψ is taken to be equal to zero at the interface and the velocity at the interface is calculated using Equation (30) expressed in terms of three-point one-sided forward differences. The vorticity at the interface and at the wall are calculated using Equation (27) and the expression below:

$$\omega = -J x_\xi v_\eta$$

These expressions at the interface and at the wall are written using a three-point one-sided forward and backward difference formulation, respectively. The boundary values are then used to recalculate the vorticity, stream function and velocity for the interior grid points. The vorticity and stream function at interior and boundary grid points are then compared with the previously calculated vorticity and stream function. If the differences are not within the specified tolerance, the calculations are repeated in an iterative manner. Once the vorticity, stream function and velocity have converged at every grid point location a new interface position is calculated as follows

$$y_{\text{new}} = y_{\text{old}} + \left(\frac{u}{v} - \frac{y_\xi}{x_\xi}\right)\Delta\xi \tag{31}$$

If the difference between y_{new} and y_{old} is not within a specified tolerance at every grid point, all calculations are repeated. Equation (31) implies that $dy/dx = u/v$ at the interface for each grid point. During the calculations λ is taken to be equal to $y_{\text{Im},1}$ which is the height or radius of the bubble at the last grid point. Since some of the boundary conditions depend on λ and λ in turn depends on the position of the interface, the boundary conditions change when the position of the interface changes. Therefore λ is replaced by $y_{\text{Im},1}$ during the calculations in order to obtain accurate results. The pressure at the interface is calculated using Equation (28) written in terms of a three-point one-sided forward difference. Also, it is not necessary to estimate the pressure at any point along the interface. The pressure at the interface could also be determined from Equation (25a) but requires an estimated pressure at the interface at the

last grid point. In other words, integrating Equation (25a) along the interface requires that $p_{\mathrm{Im},1}$ must be specified. Dutta and Ryan [29] took $p_{\mathrm{Im},1} = a/(Ca\, y_{\mathrm{Im},1}) + p_a$. In this paper, $p_{\mathrm{Im},1} = p_o - a/(Ca\, y_{\mathrm{Im},1})$ can be taken in order to estimate the pressure at the interface at the last grid point. However, in our computation it is not necessary to estimate the pressure. For the planar case $p_{\mathrm{Im},1}$ is zero since the value of the pressure in the region where the bubble becomes uniform is set equal to the constant pressure in the interior of the bubble (which has been arbitrarily set equal to zero).

Once the pressure is calculated from Equation (28), Equation (25a) is integrated numerically along the interface in order to check the correctness of the solution. In other words, the pressure drop along the x-axis at the interface was computed using Equation (28) and compared with the pressure calculated from Equation (25a). If the equation is not satisfied, the capillary number is adjusted and the computations are repeated in an iterative manner until convergence is achieved. The average of the last six grid points along the interface are selected as the convergence criterion.

As mentioned previously, the particular difficulty associated with this problem is the presence of a singularity at the origin or the nose of the bubble. From Equation (25a) when $y \to 0, \omega \to 0$, and L'Hopital's rule must be applied. In addition v is finite but $u \to 0$ when either x or $y \to 0$. Fortunately Δx or x_η does not go to zero since Δx represents a fixed distance between two grid points along the x axis. After applying L'Hopital's rule Equation (25a) becomes

$$p_\xi = Ca\lfloor(ax_\xi x_\eta J - \beta)\omega_\xi - (aJx_\xi^2 + \gamma)\omega_\eta\rfloor$$

Therefore special treatment is necessary at the beginning of the bubble in order to address the singularity.

Numerical results for two-dimensional and axisymmetric flow

Initially the interface position for a fixed bubble shape is specified. After several iterations the vorticity, stream function, and velocity converge. The new bubble shape or interface position is then calculated and computations are repeated. Convergence of the interface location and boundary conditions is typically achieved within a few iterations. Figure 5 shows the interface and grid point locations for $Ca = 3$. If the initial estimate of the interface location is nearly correct, the number of iterations will be greatly reduced. Figure 5 indicates that for $Ca = 3$ a very reasonable interface is obtained.

The pressure is calculated from Equation (28) and the pressure difference across the nose of the bubble as a function of Ca is shown in Figure 6 for planar case. As can be seen in the figure, pressure drop at the nose of the bubble as a function of capillary number differs from the results of Reinelt and Saffman [9] especially at higher capillary number. This difference can be resulted from the different equations in each paper used for calculating pressure drop. While pressure drop in the paper by Reinelt and Saffman [9] was calculated using the equation for pressure drop in the axial direction, in this paper it was computed from Equation (28) namely the normal stress boundary condition at the interface. Equation (28) is one of the three boundary conditions at the interface. The well coming stream function plots and the results concerning the fraction of liquid deposited on the walls are in good agreement with experimental data showed that the two other boundary conditions namely the tangential stress and kinematic boundary conditions at the interface were satisfied by the presented solution.

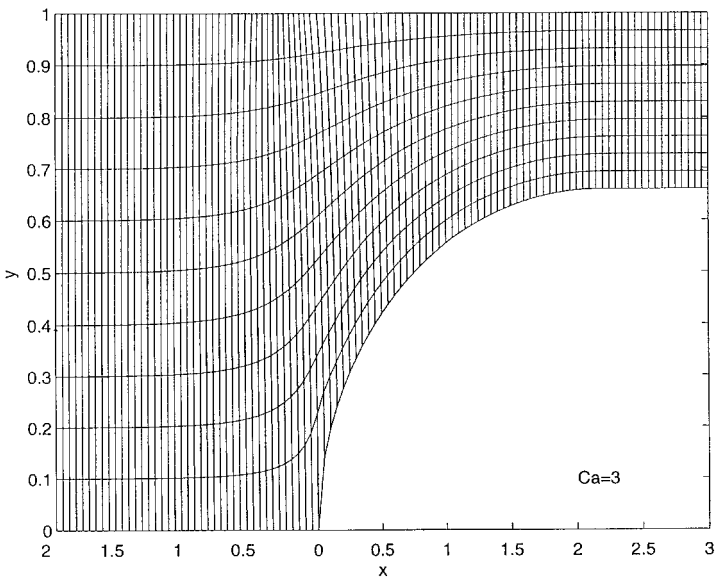

Figure 5. The calculated interface for $Ca = 3.0$.

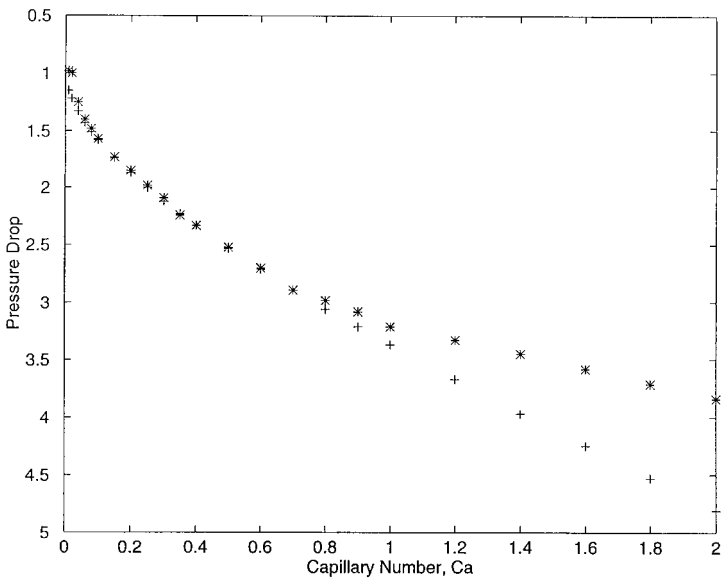

Figure 6. Pressure drop (Δp) across the nose of the bubble versus Ca for the planar numerical results (*) and the numerical results of Reinelt and Saffman ($+$).

Therefore, this disagreement concerning pressure drop at the nose of the bubble as a function of capillary number can be resulted from the calculation of the average lateral radius of the curvature computed using the modified spline-fitting method. For this calculation 101 grid points were chosen in the x-direction and 11 grid points in the y-direction ($I_m = 101$ and

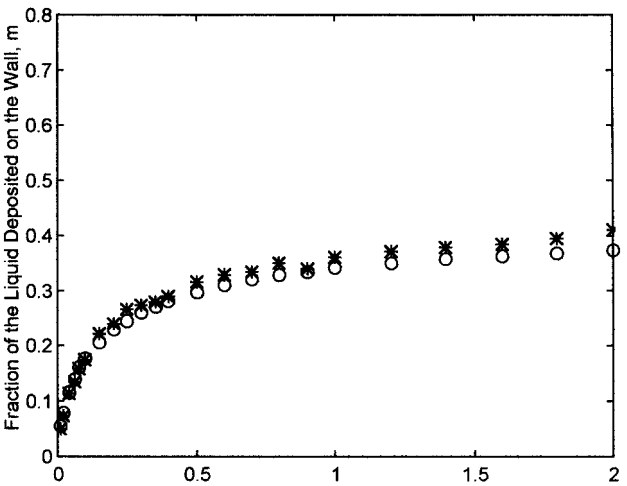

Figure 7. The fraction of liquid deposited on the wall (m) versus *Ca* for the planar numerical results (*) and numerical results of Reinelt and Saffman (○).

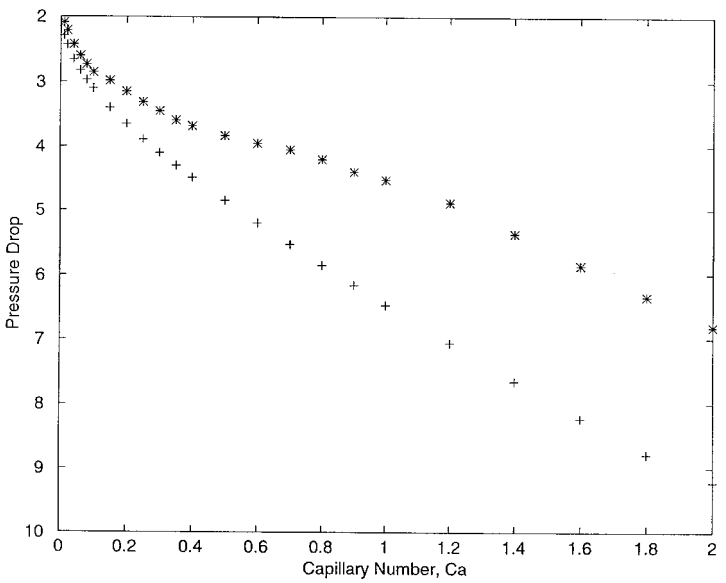

Figure 8. Pressure drop (Δp) across the nose of the bubble versus *Ca* for the axisymmetric case the numerical results (*) and the numerical results of Reinelt and Saffman (+).

$J_m = 11$). 40 grid points are used before the bubble and 60 grid points are used along the interface ($x_{min} = -2,\ x_{max} = 3$). Figure 7 shows $m = (1 - \lambda)$ versus *Ca* for the two-dimensional flow. As can be seen in Figure 7 our numerical results are in close agreement with those of Reinelt and Saffman [9] especially at lower capillary number. At higher capillary number the disagreement between our numerical data and those of Reinelt and Saffman [9] is about 8 per cent. Figure 8 is a plot of pressure versus *Ca* for the axisymmetric flow case. Figure 9 shows

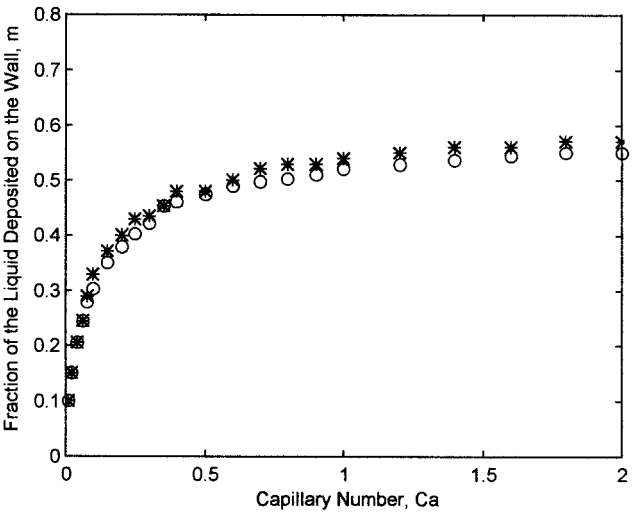

Figure 9. The fraction of liquid deposited on the wall (m) versus *Ca* for axisymmetric case the numerical results (*) and the experimental results of Taylor (○).

$m = (1 - \lambda^2)$ versus *Ca* for axisymmetric flow. Our numerical results are in close agreement with the results of Taylor [2] and our experimental data [26] at lower capillary number. The discrepancy between our numerical data and the results of Taylor [2] exists at higher capillary number.

As mentioned in the papers by Cox [4] and Reinelt and Saffman [9], for λ greater than $(1/A)^{1/(a+1)}$ the fluid near the x-axis flows away from the bubble with a higher velocity than that of the bubble (where $A = 1.5$ for the planar case and $A = 2$ for the axisymmetric case). The streamlines for those flows were discussed by Taylor [2] and Cox [4]. If λ is smaller than $(1/A)^{1/(a+1)}$, v is negative and the fluid on the x axis flows towards the bubble and there is a stagnation point at the origin.

In this method k (exponential decay rate) cannot be determined as $x \to +\infty$. However, it is not necessary to determine the value of k. The numerically calculated value of $m = (1 - \lambda)$ is given as a function of *Ca* and compared with the numerical results of Reinelt and Saffman [9] in Figure 7. The interface was obtained using Equation (31). In this paper the average lateral radius of curvature was computed using a technique similar to that employed by Reddy and Tanner [30]. The method called modified spline-fitting is employed using two neighboring surface elements along with a purely geometrical procedure.

CONCLUSION

In the present approach inertia and gravity have been neglected but can be incorporated very easily. The problem formulation is solved by using elliptic grid generation which provides flexibility for different geometry and free surface configurations. The advantages of using elliptic grid generation are the smooth grid point distribution, one-to-one transformation, and

the fact that complex boundary conditions are easily treated. The grid construction takes very little time in comparison with the time for calculating the interface of the gas-assisted displacement problem.

In this method an accurate determination of the fraction of liquid deposited on the walls of the channel can be obtained. In this approach, the bubble shape and flow field are a weak function of the capillary number although experiments indicate that the effect of capillary number is very important in determining the shape of the bubble. The region near the nose of the bubble needs to be treated in a special way due to the presence of a singularity. The pressure drop across the bubble front increases with increasing capillary number for both the planar and axisymmetric case. The results of the numerical solution are in very good agreement with the experimental data.

REFERENCES

1. Fairbrother F, Stubbs AE. Studies in electroendosmosis. Part VI. The bubble-tube methods of measurements. *Journal of Chemical Society* 1935; **1**:527.
2. Taylor GI. Deposition of a viscous fluid on the wall of a tube. *Journal of Fluid Mechanics* 1961; **10**:161.
3. Cox BG. On driving a viscous fluid out of a tube. *Journal of Fluid Mechanics* 1962; **14**:81.
4. Cox BG. Experimental investigation of the streamlines in viscous fluid expelled from a tube. *Journal of Fluid Mechanics* 1964; **20**:193.
5. Bretherton FP. The motion of long bubbles in tubes. *Journal of Fluid Mechanics* 1961; **10**:166.
6. Schwart LW, Princen HW, Kiss AD. On the motion of bubbles in capillary tubes. *Journal of Fluid Mechanics* 1986; **172**:259.
7. Marchessault RH, Mason SG. Flow of entrapped bubbles through a capillary. *Industrial Engineering Chemistry* 1960; **52**:79.
8. Park CW, Homsy GM. Two phase displacement in Hele-Shaw cell. *Journal of Fluid Mechanics* 1984; **139**:291.
9. Reinelt DA, Saffman PG. The penetration of a finger into a viscous fluid in a channel and tube. *SIAM Journal of Science and Statistical Computers* 1985; **6**:542.
10. Shen EI, Udell KS. A finite element study of low Reynolds number two phase flow in cylindrical tubes. *Transactions of the ASME E*: *Journal of Applied Mechanics* 1985; **52**:253.
11. Ratulowski J, Chang HC. Transport of gas bubbles in capillaries. *The Physics of Fluids A* 1989; **1**:1642.
12. Kolb WB, Cerro RL. Coating the inside of a capillary of square cross-section. *Chemical Engineering Science* 1991; **46**:2181.
13. Kolb WB, Cerro RL. The motion of long bubbles in tubes of square cross-section. *The Physics of Fluids A* 1993; **5**:1549.
14. Poslinski AJ, Oehler PR, Stokes VK. Isothermal gas-assisted displacement of viscoplastic liquids in tubes. *Polymer Engineering and Science* 1995; **35**:877.
15. Ro TS, Homsy GM. Viscoelastic free surface flows: thin film hydrodynamics of Hele-Shaw and dip coating flows. *Journal of Non-Newtonian Fluid Mechanics* 1995; **57**:203.
16. Saffman PG, Taylor GI. The penetration of a fluid into a porous medium or Hele-Shaw cell containing a more viscous liquid. *Proceedings of Royal Society of London A* 1958; **245**:312.
17. Pitts EJ. Penetration of a fluid into Hele-Shaw cell: the Saffman-Taylor Experiment. *Journal of Fluid Mechanics* 1980; **97**:53.
18. Tabelling P, Zocchi G, Libchaber A. An experimental study of the Saffman-Taylor instability. *Journal of Fluid Mechanics* 1987; **177**:67.
19. McLean JM, Saffman PG. The effect of surface tension on the shape of fingers in a Hele-Shaw cell. *Journal of Fluid Mechanics* 1981; **102**:455.
20. Landau LD, Levich VG. Dragging of a liquid by moving plate. *Acta Physicochimica URSS* 1942; **17**:42.
21. Reinelt DA. The effect of thin film variations and transverse curvature on the shape of fingers in Hele-Shaw cell. *The Physics of Fluids* 1987; **30**:2617.
22. Reinelt DA. Interface conditions for two-phase displacement in Hele-Shaw cells. *Journal of Fluid Mechanics* 1987; **183**:219.
23. Taylor GI. Cavitation of a viscous fluid in narrow passages. *Journal of Fluid Mechanics* 1963; **16**:595.
24. Fernandes RC, Semiat R, Dukler EA. Hydrodynamic model for gas-liquid slug flow in vertical tube. *AIChE Journal* 1983; **29**:981.
25. Kolb WB, Papadimitriou AA, Cerro RL. The ins and outs of coating monolithic structures. *Chemical Engineering Progress* 1993; **89**:61.

26. Kamişli F. Mathematical analysis and experimental study of gas-assisted injection molding. *Ph.D. Dissertation*, State University of New York at Buffalo, 1997.
27. Thompson JF, Thames FC, Mastin CW. Automatic Numerical generation of body-fitted curvilinear coordinates system for field containing any number of arbitrary two-dimensional bodies. *Journal of Computational Physics* 1974; **15**:299.
28. Hoffman KA, Chang ST. *Computational Fluid Dynamics for Engineers*, vol. 1. Engineering Educational System: Wichita, Kansas, 1995.
29. Dutta A, Ryan ME. Dynamics of a creeping Newtonian jet with gravity and surface tension: a finite difference technique for solving steady free surface flows using orthogonal curvilinear coordinates. *AIChE Journal* 1982; **28**:220.
30. Reddy KR, Tanner RI. Finite element solution of viscous jet flows with surface tension. *Computers and Fluids* 1978; **6**:83.

